

# Syllectometry: The Effect of Aggregometer Geometry in the Assessment of Red Blood Cell Shape Recovery and Aggregation

Johannes G. G. Dobbe\*, Geert J. Streekstra, Jan Strackee, Marcel C. M. Rutten, Johannes M. A. Stijnen, and Cornelis A. Grimbergen

**Abstract**—Syllectometry is a measuring method that is commonly used to assess red blood cell (RBC) aggregability. In syllectometry, light is incident on a layer of whole blood initially exposed to shear flow. The backscattered light is measured after abruptly stopping the driving mechanism. The resultant time-dependent intensity plot is called the syllectogram. Parameters that quantify RBC aggregability are obtained by analyzing the syllectogram. As we will show in this paper, the upstroke in the initial part of the syllectogram contains the information for measurement of RBC-shape recovery in whole blood as well.

To estimate RBC-shape recovery, we extended the existing two-exponential mathematical representation of the syllectogram by a third exponent that describes the upstroke. To investigate the feasibility of RBC-shape recovery measurement from the upstroke, we derived an analytical model of the flow decay that follows after abruptly stopping the driving mechanism. The model reveals that for large gaps the flow decay may interfere with the true RBC-shape recovery process. These theoretical findings were confirmed by velocity measurements in a Couette-type aggregometer.

Syllectograms obtained using large gaps differ in many respects from those obtained using small gaps. As predicted by our model large gaps show a prolonged apparent shape-recovery time-constant. Moreover, a delayed intensity peak, a reduced upstroke of the intensity peak and a considerable increase of the half-life parameter are observed. The aggregation indices for large gaps are lower than for small gaps.

This paper yields a better understanding of the velocity and shear-rate decay following upon abruptly stopping the driving mechanism. A better mathematical representation of the syllectogram and recommendations for a maximum gap width enables both RBC-shape recovery and aggregation measurements in whole blood using syllectometry.

**Index Terms**—Aggregation, red blood cell, relaxation, shape recovery, syllectogram, syllectometry, velocity decay.

Manuscript received April 25, 2002; revised July 25, 2002. Asterisk indicates corresponding author.

\*J. G. G. Dobbe is with the Department of Medical Technological Development, Academic Medical Center, University of Amsterdam, P.O. Box 22700, 1100 DE Amsterdam, The Netherlands (E-mail: j.g.dobbe@amc.uva.nl).

G. J. Streekstra is with the Department of Medical Physics, Academic Medical Center, University of Amsterdam, 1100 DE Amsterdam, The Netherlands.

J. Strackee, retired, can be reached through the Department of Medical Physics, Academic Medical Center, University of Amsterdam, 1100 DE Amsterdam, The Netherlands.

C. A. Grimbergen is with the Department of Medical Physics and the Department of Medical Technological Engineering, Academic Medical Center, University of Amsterdam, 1100 DE Amsterdam, The Netherlands.

M. C. M. Rutten and M. J. M. A. Stijnen are with the Department of Biomedical Engineering, Eindhoven University of Technology, 5612 AZ Eindhoven, The Netherlands.

Digital Object Identifier 10.1109/TBME.2002.807319

## I. INTRODUCTION

THE viscosity of blood at low shear rates is mainly determined by red blood cell (RBC) aggregation. This property of RBCs is found increased in a number of diseases, such as inflammatory diseases, diabetes, thrombosis and myocardial infarction [1]. Syllectometry as originally described by Zijlstra [2], [3] is commonly employed to measure RBC aggregability in research studies [3]–[13]. It provides parameters reflecting the extent of aggregation but also parameters describing the kinetics of aggregate formation. The method is fast, in contrast to erythrocyte sedimentation tests [14], [15], and accurate [9] and has high potential for assessing RBC aggregation in a clinical setting.

In syllectometry, blood is illuminated and subjected to a shear rate, high enough to fully disaggregate the cells and to elongate them in the direction of the flow [5], [13]. The backscattered light is measured after the driving mechanism stops. The resultant time-dependent intensity plot is called a syllectogram (see Figs. 4 and 12). A high-intensity peak shows up at the beginning of the plot as cells return to their original randomly oriented biconcave shape and lose their alignment. The intensity of the backscattered light decreases as aggregation proceeds. A two-exponential mathematical representation of the syllectogram yields aggregation parameters that are used to assess RBC aggregability [5], [8]–[12].

Besides biological differences between individual blood samples, the geometry of the aggregometer may also influence the shape of the syllectogram. This issue has not yet been addressed in the literature but may result in a misinterpretation of the derived aggregation parameters. The intensity of the backscattered light increases with the number of scattering particles and, therefore, with the size of the gap [16], effectively leading to an increase of the syllectogram intensity scale. Moreover, mass inertia of the suspension increases with the size of the gap, which causes a prolongation of the shear-rate decay after stopping the driving mechanism. This is expected to influence RBC-shape recovery and the time before the occurrence of the peak, in the syllectogram.

In this paper, we extend the existing two-exponential syllectogram representation with a third exponent to include the initial upstroke attributed to RBC-shape recovery and investigate the possibility to measure RBC-shape recovery using syllectometry. For that purpose we present a mathematical model that describes the suspension velocity and shear-rate decay in aggregometers

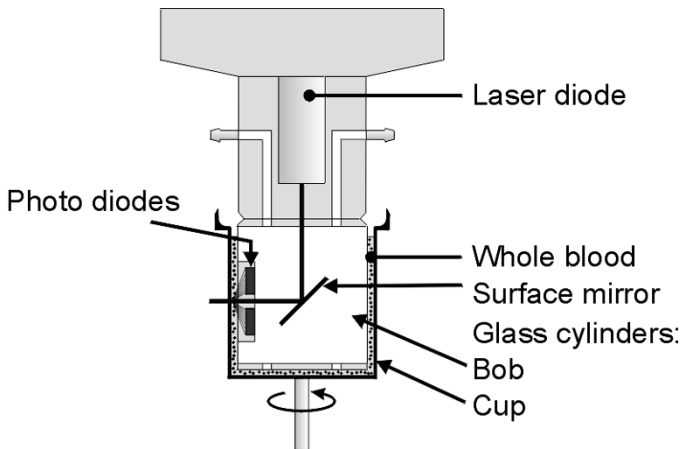


Fig. 1. LORCA aggregometer setup. A laser beam is incident on a layer of blood between a static inner cylinder (bob) and a rotating outer cylinder (cup). Backscattered light is collected by two photo diodes.

following upon abruptly stopping the driving mechanism. Our model is derived from the Navier–Stokes equations for one-dimensional (1-D) flow in a narrow gap. The model is validated using particle image velocimetry (PIV) [17]. The mathematical model is subsequently used to study the influence of a prolonged RBC-shape recovery—due to flow decay—on aggregation parameters that are derived from the syllectogram. The results help us to gain a better understanding of the physics and biomechanics behind syllectometry and to allow for a recommendation for the maximum gap width to be used in syllectometry.

## II. MATERIALS AND METHODS

### A. Experimental Setup

The experiments are carried out with the LORCA Couette aggregometer [9], as depicted in Fig. 1. A laser beam (670 nm) is incident on a layer of blood between a static inner cylinder (the bob, radius = 15.7 mm) and a rotating outer cylinder (the cup). Four different highly polished Plexiglas cups were used, resulting in gap widths of 0.37, 0.60, 1.05, and 2.00 mm. Light that is backscattered by the layer of blood in the gap is collected by two photodiodes inside the static bob and is converted into an electrical signal. After cup rotation cessation, the electrical signal is sampled for 120 s at 250 Hz using the analog-to-digital converter board of a personal computer. The data are stored to disk for off-line analysis.

Mass inertia and elasticity of the mechanical parts cause the cup to behave as a second-order system that exhibits ringing in response to motor cessation. To damp residual oscillatory motion, the commercial system was augmented by a simple brake mechanism, consisting of a cotton belt strained around the spindle that drives the cup.

### B. Flow Decay

1) *Modeling the Velocity and Shear-Rate Decay:* A Couette geometry is used to create a shear rate that is virtually uniform over the gap, provided that the bob radius is large in relation to the gap width. To simplify the calculation of the velocity decay  $u(y, t)$  ( $y$ : distance to the bob,  $t$ : time) following cup cessation, the Couette geometry is approximated by a parallel plate system [Fig. 2(a)].

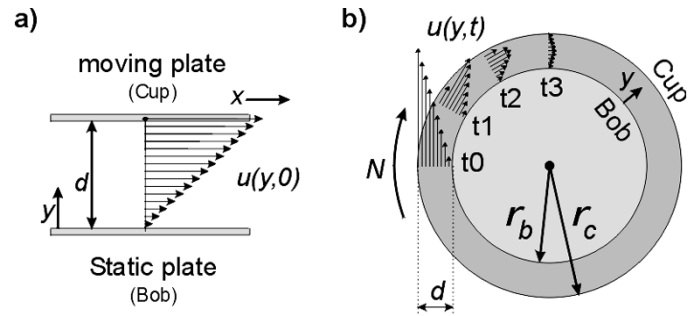


Fig. 2. (a) The upper plate of a parallel plate system moves at constant speed  $u_0$  in the  $x$ -direction to invoke a proportional velocity profile  $u(y, t)$  approximating the flow in a Couette system if the cup rotates at the same (tangential) velocity  $u_0$ . (b) Suspension inertia causes the velocity to slowly decay after abrupt cessation of the cup at  $t = 0$  (for clarity, the profiles at  $t_0 \dots t_3$  are drawn at different locations).

In this parallel plate system, a simple shear flow is obtained by moving the upper plate with respect to the static lower plate in the  $x$ -direction at a constant speed  $u_0$ . In this configuration, the shear rate equals  $\gamma_0 = du/dy = u_0/d$ , where  $d$  is the distance between the plates. In a Couette system, the stationary shear rate (during rotation) is not uniformly distributed over the gap as in a parallel plate system. If the tangential velocity of the outer cup in the Couette system is taken equal to the velocity of the moving plate in a parallel plate system, a small deviation results. In the present experimental setup, this deviation ranges between +6% and –17% for the largest gap (2 mm) and decreases roughly proportionally with the gap width. The exact magnitude of the shear rate deviation is of lesser importance since we are mainly interested in the general behavior of the velocity-decay time in response to abrupt cup cessation [see Fig. 2(b)].

In a non-Newtonian suspension like blood, viscosity changes with shear rate [18] and is affected by RBC deformation and aggregation. The viscosity does not change instantly following cup cessation because the cells need time to reshape and to form aggregates. Viscosity changes are, therefore, considered negligible during velocity decay. Thus, the velocity decay following cup cessation is calculated for a Newtonian fluid in the approximately equivalent parallel-plate system. The partial differential equation for this 1-D viscous-flow problem without pressure gradient is obtained from the Navier–Stokes equation for a Newtonian fluid [19], which reduces to

$$\frac{\partial u(y, t)}{\partial t} = v \frac{\partial^2 u(y, t)}{\partial y^2} \quad (1)$$

with  $v$  the kinematic viscosity ( $v = \eta/\rho$ , with  $\eta$  the dynamic viscosity and  $\rho$  the density) of the suspension. The solution of the velocity decay  $u(y, t)$  and shear-rate decay  $\gamma(y, t)$  in the absence of cup ringing are found with the appropriate initial and boundary conditions and yields (see Appendix

$$u(y, t) = -u_0 \frac{2}{\pi} \sum_{n=1}^{\infty} \frac{(-1)^n}{n} \sin\left(\frac{n\pi y}{d}\right) \cdot e^{-\left(\frac{n\pi}{d}\right)^2 vt} \quad (2a)$$

$$\gamma(y, t) = -2\gamma_0 \sum_{n=1}^{\infty} (-1)^n \cos\left(\frac{n\pi y}{d}\right) \cdot e^{-\left(\frac{n\pi}{d}\right)^2 vt} \quad (2b)$$

with  $u_0$  the initial tangential cup velocity,  $\gamma_0$  the initial shear rate and  $d$  the gap width.

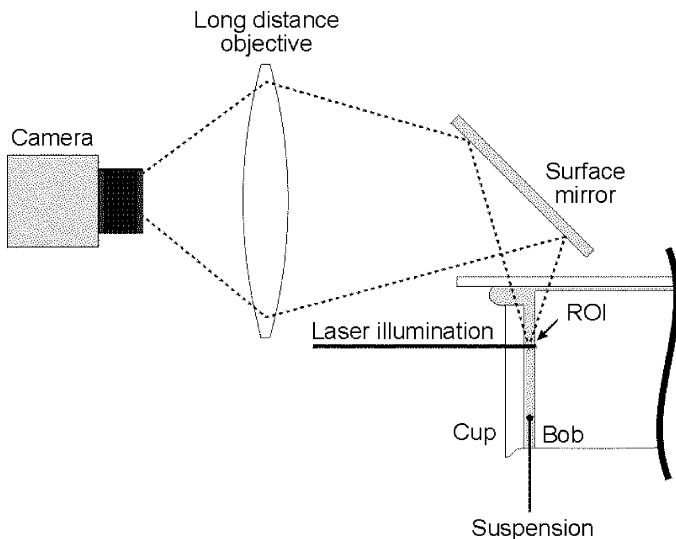


Fig. 3. Velocity measurement using PIV. A camera focuses on a laser-illuminated region of interest (ROI) between the static bob and the rotating cup. The velocity of seeding particles in the ROI is repeatedly determined based on their displacement in image-pairs with a known interimage delay.

In practice, mass inertia and the driving mechanism's elasticity should be taken into account that cause ringing of the cup in response to motor cessation. The ringing effect superimposes an oscillation on the smoothly decaying fluid velocity. The appendix shows that ringing adds two additional terms to (2a) and (2b).

2) *Velocity-Decay Measurement Procedure*: PIV (PIV 1100, Dantec, Skovlunde, Denmark) [17] was used to verify the theoretical velocity decay in the Couette system (bob radius = 15.7 mm, gap width = 1 mm, see Fig. 3). With this technique a camera is positioned parallel to the axis of rotation and focuses on a selected suspension layer. Two successive laser-illuminated images are acquired with a known interimage delay. The displacement of suspended particles in each picture-pair depends on local velocity and is obtained by correlation techniques. By periodically determining local fluid velocities from image-pairs, one obtains the velocity versus time at multiple locations in the fluid.

A long-distance objective (numerical aperture = 0.1) was focused on a laser-illuminated suspension layer containing light scattering seeding particles (polyamid,  $\varnothing = 20 \mu\text{m}$ ). The focal plane was approximately 2 mm below the surface. The suspension surface was covered with a glass plate to reduce optical disturbances. The small clearance (approximately 0.5 mm) between the glass cover plate and the top of the rotating cylinder was bridged by the suspension.

The seeding particles were suspended in water ( $\nu = 10^{-6} \text{ m}^2/\text{s}$ ). The viscosity of water is about four times lower than that of blood at a shear rate of  $400 \text{ s}^{-1}$ , which is of advantage because it slows down the process and eases measuring the flow decay using PIV. The interimage delay for any given pair was 1.5 ms. Image-pairs were taken every 6.66 ms (sample rate 150 Hz) for a period of 200 ms. A mechanical brake mechanism was utilized to reduce the effect of mechanical ringing. The velocities in the gap were plotted versus the distance to the bob ( $y$ ) and versus the time ( $t$ ). The

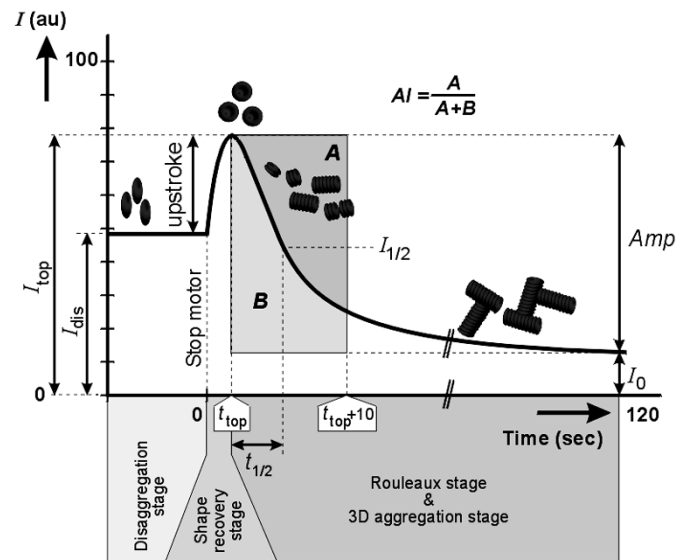


Fig. 4. The syllectogram distinguishes four behavioral stages: 1) disaggregation, 2) RBC-shape recovery, 3) rouleaux formation, immediately followed by 4) 3-D aggregate formation. The peak duration is exaggerated. au = arbitrary units.

velocity profile was smoothed by applying a two-dimensional Gaussian kernel.

### C. Syllectogram Description

In a syllectogram, four RBC-behavioral stages are distinguished (Fig. 4). These are as follows. 1) The initial plateau during the disaggregation stage originates from the light that is backscattered by the elongated RBCs that are aligned in the direction of the flow. The intensity of the light relates to the state of elongation and, thus, depends on the shear rate. 2) In the shape-recovery stage that follows immediately after cup cessation, cells collectively lose their alignment and return to their biconcave resting shape. The recovery stage is accompanied by an exponential increase in light backscatter [20] leading to a high-intensity peak in the syllectogram. 3) Aggregation starts during the shape-recovery stage when external shear forces fail to keep the RBCs dissociated. RBCs start to aggregate side-to-side as stacks of coins, called rouleaux, causing the backscatter of light to decrease exponentially [6] with a time-constant of about 1–3 s in normal human blood. 4) Rouleaux formation is immediately followed by so-called three-dimensional (3-D) aggregate formation during which rouleaux connect end-to-end as well as side-to-end, creating larger 3-D aggregates. In normal human blood, the formation of 3-D aggregates is a slower process [8] with a time-constant of about 10–25 s.

1) *Triexponential Syllectogram Representation*: The conventional mathematical representation of the syllectogram contains two time-constants and describes the curve from the peak onward [8]–[10]. This paper introduces a third time-constant to include the upstroke caused by RBC shape recovery [20]. Thus, the intensity curve  $I(t)$  was fitted using a triexponential function containing three time-constants associated with RBC-shape recovery ( $T_r$ ), rouleaux formation ( $T_f$ ) and 3-D aggregate formation ( $T_s$ )

$$I(t) = -I_r \cdot e^{-t/T_r} + I_f \cdot e^{-t/T_f} + I_s \cdot e^{-t/T_s} + I_0 \quad (3)$$

where  $I_r$ ,  $I_f$  and  $I_s$  denote the contribution of shape recovery, (fast) rouleaux formation, and (slow) 3-D aggregate formation, respectively.

The curve fit is performed using the Levenberg-Marquardt algorithm [21] for fitting nonlinear functions. Since the syllectogram is sampled uniformly, most data points stem from the tail of the curve. To prevent the fitting algorithm from focusing on this region, the curves were re-sampled by selecting 500 points uniformly distributed on a logarithmic time scale.

Several aggregation parameters are derived from the syllectogram as indicated in Fig. 4. The amplitude (*Amp*) is used to describe the extent of aggregation [8], [9]. Aggregation kinetics is described by the time-constants  $T_f$  and  $T_s$  but also by  $t_{1/2}$ . The latter is the time that elapses until the peak intensity is reduced by half the amplitude (to  $I_{1/2}$ ). In clinical hemorheology, a single parameter is sometimes used to describe the overall aggregation behavior of the suspension. This aggregation index (AI) is a value between zero and one and depends on both the extent and kinetics of aggregation [5], [7]–[9]. It is often determined from the areas  $A$  and  $B$  bounded by  $t = t_{\text{top}}$  and  $t = t_{\text{top}} + 10$  s as  $\text{AI} = A/(A + B)$  (see Fig. 4) [9].

The time elapsed until the occurrence of the peak is sometimes used as an indication of the RBC-shape recovery time. The peak occurs when the first derivative of (3) equals zero. The first derivative depends on *all* parameters of (3) including the aggregation parameters. The fact that  $t_{\text{top}}$  is influenced by the aggregation process makes it an unsuitable candidate for representing the RBC-shape recovery time.

2) *Measuring the Effect of Aggregometer Geometry:* The effect of the aggregometer geometry on the syllectogram and its parameters was investigated by varying the gap width (0.37, 0.60, 1.05 and 2.00 mm). The triexponential syllectogram representation was first evaluated and then applied to determine the deviations in syllectogram time parameters ( $T_r$ ,  $t_{\text{top}}$ ,  $T_f$ ,  $T_s$ ,  $t_{1/2}$ ) and intensity parameters (Upstroke, *Amp*, AI) in different gaps.

Syllectograms of eight individuals were measured using four different gaps: 0.37, 0.60, 1.05, and 2.00 mm. A fresh sample was used after each cup change. In the following, the two-tailed paired t-test was used to test the null hypothesis of equal means.

#### D. Blood-Sample Preparation

Blood samples, 25 ml each, of eight healthy donors were collected from the antecubital vein using ethylene diamine-tetraacetic acid (EDTA) as anticoagulant. Since backscattering depends on the level of oxygenation, the blood samples were fully oxygenated before each experiment [9]. The volume fraction of RBCs was in the range of 0.44–0.46 l/l. A syllectogram was measured after disaggregating the blood sample at a shear rate of  $400 \text{ s}^{-1}$  for 10 s. Measurements were performed within 1–6 hours after blood withdrawal.

### III. RESULTS

#### A. Flow Decay

1) *Theoretical Considerations of the Flow Decay:* Fig. 5 displays in three dimensions the normalized velocity [Fig. 5(a)] and shear rate [Fig. 5(b)] decay in the absence of cup ringing. The parameters  $u$ ,  $\gamma$  and  $y$  are normalized ( $u/u_0$ ,  $\gamma/\gamma_0$ , and

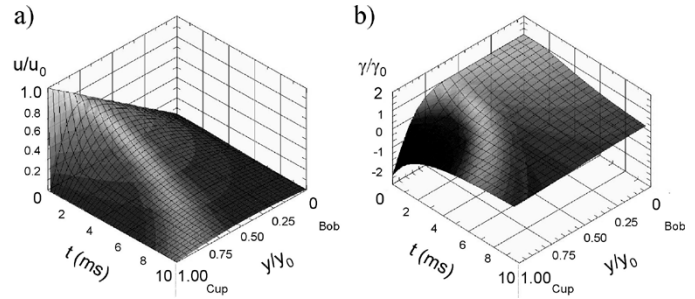


Fig. 5. (a) Relative velocity profile and (b) shear rate profile between bob and cup following cup cessation. No cup ringing;  $d = 0.37$  mm;  $v$  of normal human blood at  $400 \text{ s}^{-1}$ .

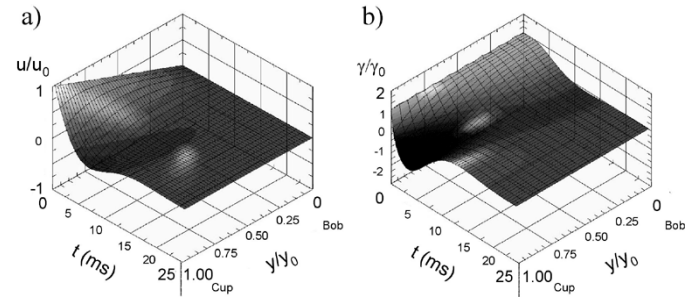


Fig. 6. Typical example of the (a) relative velocity profile and (b) shear rate profile between bob and cup following cup cessation. Damped cup ringing (50 Hz, time-constant = 5 ms);  $d = 0.37$  mm;  $v$  of normal human blood at  $400 \text{ s}^{-1}$ .

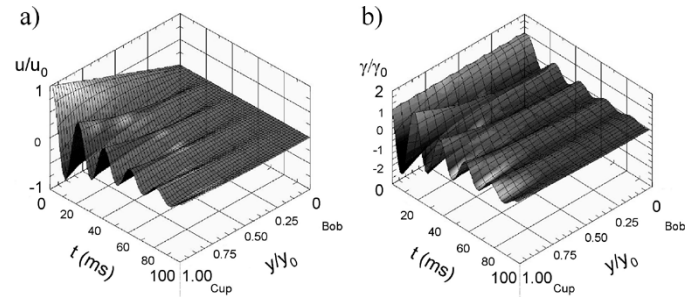


Fig. 7. (a) Relative velocity profile and (b) shear rate profile between bob and cup following cup cessation. Undamped cup ringing (50 Hz, time-constant = 40 ms);  $d = 0.37$  mm;  $v$  of normal human blood at  $400 \text{ s}^{-1}$ . The profiles in this figure characterize the commercial LORCA aggregometer [9].

$y/d$ , respectively). In this particular instance, the kinematic viscosity was that of normal human blood at a shear rate of  $400 \text{ s}^{-1}$ , being  $3.8 \cdot 10^{-6} \text{ m}^2/\text{s}$  [18]. The smallest gap width (0.37 mm) was considered. Fig. 5(b) illustrates that the shear rate reverses and rises sharply in the vicinity of the cup immediately after cup cessation.

Fig. 6 shows the effect of damped oscillatory motion of the cup (50 Hz, time-constant = 5 ms) for the same geometry as in Fig. 5. In Fig. 7, the damping is reduced (time-constant = 40 ms), clearly revealing the effect of oscillatory motion. Fig. 7 characterizes the commercial LORCA aggregometer [9].

It appears from Fig. 5–7 that the shear rate is not uniformly distributed over the gap *during the velocity decay*. If layers of fixed width represent the blood in the gap, then RBCs in each layer are in a different state of shape recovery and/or aggregation after cup cessation yielding different contributions to the syllectogram. In addition, cells in close vicinity of the bob give

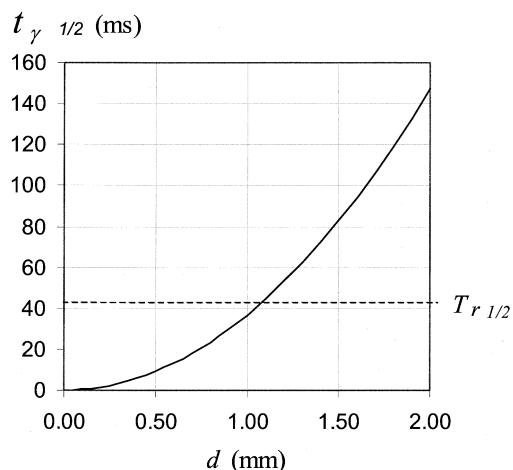


Fig. 8. The shear-rate half-life ( $t_{\gamma,1/2}$ ) at the bob in normal human blood versus the gap width ( $d$ ) after shearing at  $400 \text{ s}^{-1}$ . The dotted line indicates the typical half-life value ( $T_{r,1/2}$ ) of RBC-shape recovery [20].

a larger contribution to the intensity of the backscattered light than distant cells do [16]. The net result is a gap-width dependent syllectogram.

The shear rate is the actual parameter affecting RBC deformation and aggregation. The shape recovery of cells can only be measured if the shear rate decays faster than do cells recover their biconcave resting shape. The shear-rate decay happens to be slowest in the vicinity of the bob [Fig. 5(b)] where cells' contribution to the backscatter intensity is the highest [16]. It is, therefore, appropriate to investigate the shear-rate decay at the bob. Since it is not possible to describe the shear-rate decay by a single time-constant as can be seen from (2b), a half-life parameter was used. The half-life depends on the gap width ( $d$ ) and is defined as the time required for the shear rate to reduce by 50% of its initial value. Equation (2b) was used to numerically determine the shear-rate half-life  $t_{\gamma,1/2}(d)$  (by solving  $\gamma(0, t_{\gamma,1/2}) = 0.5$ ) at the bob in normal human blood [18] ( $\nu = 3.8 \cdot 10^{-6} \text{ m}^2/\text{s}$  at  $\gamma = 400 \text{ s}^{-1}$ ), see Fig. 8.

A shape-recovery half-life of  $T_{r,1/2} = 43 \text{ ms}$  has been reported for human RBCs in a phosphate-buffer saline/dextran solution of similar kinematic viscosity [20]. Fig. 8 shows that the shear-rate half-life exceeds the RBC-shape recovery half-life for  $d > 1.1 \text{ mm}$ , resulting in a prolongation of the observed RBC-shape recovery time as measured from the syllectogram (see Section II-D).

2) *Flow-Decay Measurement*: The theoretical velocity-decay profile in a 1-mm gap filled with water is depicted in Fig. 9(a) and is accompanied by that measured using PIV in Fig. 9(b). To be able to evaluate the measured velocity profile with the theoretical curves, we compared cross sections of the 3-D graphs in Fig. 9. Fig. 10(a) shows these cross sections at values of  $t$  equal to 0, 20, 60, and 120 ms. Fig. 10(b) shows cross sections at values of  $y/y_0$  equal to 0.22, 0.50 and 0.77. Both figures demonstrate that the velocity profiles [Fig. 10(a)] and the velocity-decay curves [Fig. 10(b)] closely match the theoretical curves (dotted lines) despite a deviation close to the cup immediately following cup cessation. The deviation is due to optical deflections at the cylinder walls and to residual mechanical ringing. Taking these sources of deviation into consideration we conclude that the theoretical

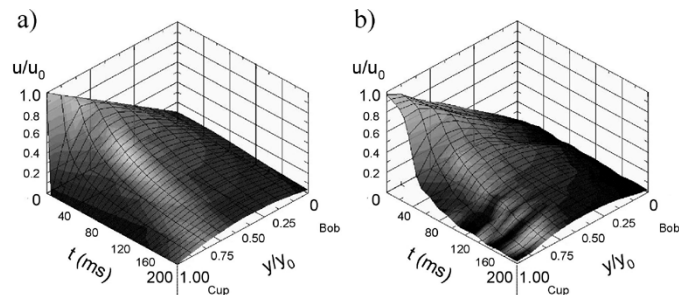


Fig. 9. Velocity decay of water in a Couette system after cup cessation: (a) theoretical and (b) measured using PIV. Bob radius = 15.7 mm; gap width = 1 mm.

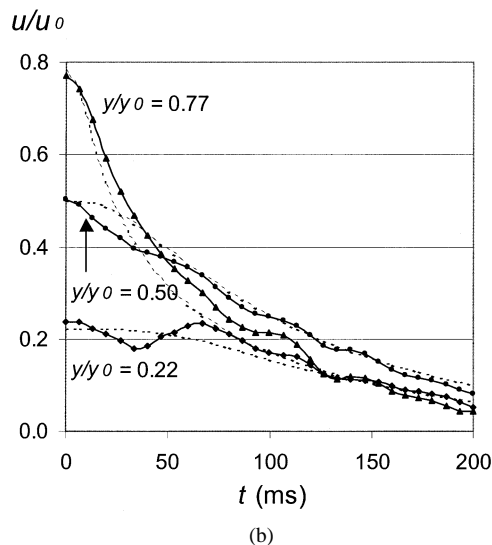
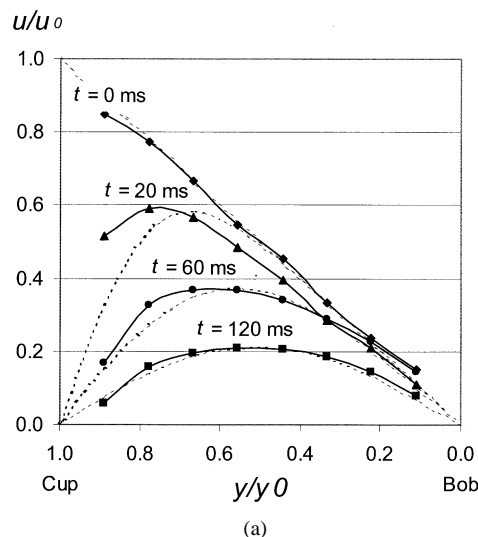


Fig. 10. Cross sections of Fig. 9 showing: (a) velocity profile between bob ( $y/y_0 = 0$ ) and cup ( $y/y_0 = 1$ ) at different time points and (b) Velocity-decay curves at different locations. The dotted lines represent the theoretical curves.

model provides a fairly good representation of the velocity and shear-rate decay in the gap.

## B. Syllectogram Measurements

1) *Validation of Triexponential Syllectogram Representation*: The validity of three mathematical syllectogram

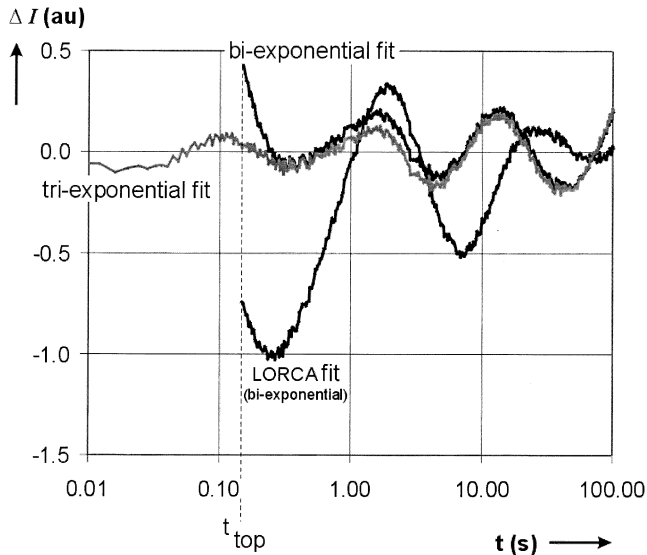


Fig. 11. Deviation ( $\Delta I$ ) between mathematical syllectogram representations and a measured curve. au = arbitrary units.

representations were assessed by comparing them against the measured syllectogram [e.g., Fig. 12(a)] of a healthy volunteer (0.37-mm gap). The measured curve was first fitted using the biexponential curve strip method implemented in the LORCA [8], [9]. The same syllectogram was then fitted to the biexponential and triexponential representations of the syllectogram using the Levenberg-Marquardt fitting algorithm [21]. The biexponential representations excluded the RBC-shape recovery term ( $I_r$ ,  $T_r$ ).

Fig. 11 shows the difference ( $\Delta I$ ) between the mathematical representations and the measured curve. The use of a logarithmic time-scale provides a better view of the deviation over the entire curve but falsely gives the impression of signal oscillation. The measured curve actually swings only 0.25% of the full scale (0–100 au) around the biexponential and triexponential curves as is seen on the enlarged vertical scale of Fig. 11. The figure demonstrates that, in the first few seconds, the triexponential syllectogram representation matches the measured curve more closely than the biexponential variants. This justifies the use of the triexponential representation for studying RBC-shape recovery in small gaps. The triexponential fit also proves useful for studying the effect of the shear-rate decay on the shape of the entire syllectogram in the case of larger gaps as well (see Fig. 12).

2) *The Effect of Aggregometer Geometry on Syllectogram Parameters:* Syllectograms of a single individual obtained using the four different gap widths indicate [Fig. 12(a)] that backscatter intensity increases with the gap width. The dots represent the syllectogram, while the solid lines represent the triexponential fit. An enlargement of the syllectogram peak [Fig. 12(b)] reveals that the peak is delayed and that the fit deviates from the measurement for gaps larger than 0.6 mm. The most prominent delay is observed for the 2-mm gap, which is consistent with the theoretical shear-rate half-life ( $\approx 150$  ms, see Fig. 8). Fig. 12(b) also shows that, as the gap width increases, the peak amplitude decreases while the overall backscatter intensity increases.

The histogram of Fig. 13(a) shows the shape recovery time-constant  $T_r$  and the time until the occurrence of the peak  $t_{top}$ , for

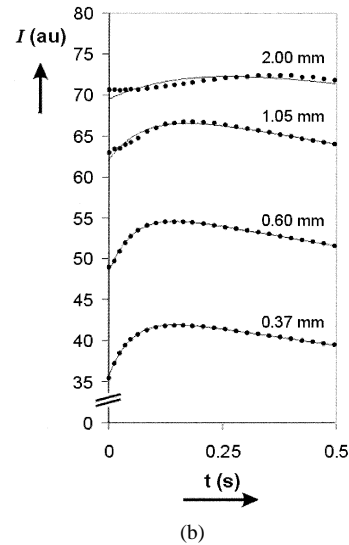
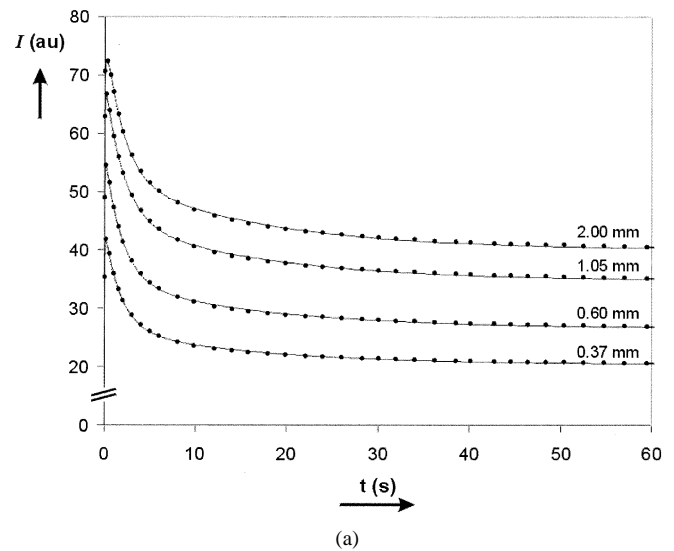


Fig. 12. (a) First 60 s of syllectograms of one healthy volunteer measured using four different gaps. The dots indicate the measured syllectograms while the solid lines represent the triexponential fit. (b) First 500 ms of the syllectogram show the deviation of the fit for large gaps. au = arbitrary units.

different gaps. It illustrates that the 0.60-mm gap has virtually the same time constant ( $P > 0.05$ ) as the 0.37-mm gap. The important increase ( $P < 0.05$ ) in the shape-recovery time for large gaps is explained by the fact that the shear-rate half-life is close to the RBC-shape recovery half-life in these gaps (see Fig. 8). The intensity peak occurs at a different time point  $t_{top}$  for all gaps larger than 0.37 mm ( $P < 0.05$ ) although a major delay is only observed in the case of the 2-mm gap. Fig. 12(b) shows that the triexponential fit underestimates the true delay for large gaps ( $>1$  mm).

To determine the change in syllectogram parameters for gaps  $>0.37$  mm, the estimated parameters for a 0.37-mm gap was taken as reference. The data was normalized by taking the ratio of each estimated parameter and its reference value, which yielded a series of relative time parameters. This enabled the data to be represented in a single cumulative graph [Fig. 13(b)]. As can be seen in Fig. 13(b), for larger gaps, the aggregation time-constants  $T_f$  and  $T_s$  are different ( $P < 0.05$  for the 0.60- and 1.05-mm gaps) although the effect is rather small.

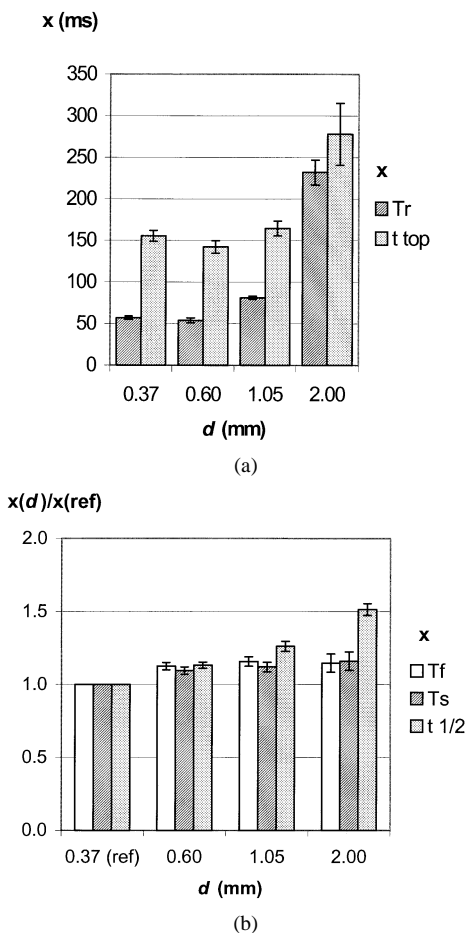


Fig. 13. (a) The recovery time-constant  $T_r$  and  $t_{top}$  for different gap widths ( $d$ ). (b) Changes in kinetic aggregation-parameter estimates obtained by triexponential fitting of the syllectograms. Results of the 0.37-mm gap served as reference. The error bars indicate the standard error of the mean ( $N = 4$  for the 2-mm gap,  $N = 8$  for all other gaps).

This is an important finding since it allows comparing  $T_f$  and  $T_s$  parameters obtained from aggregometers with different gaps. An increased shear-rate decay time is accompanied by a decrease in peak intensity [see Fig. 12(b)]. This causes the half-life parameter  $t_{1/2}$  to increase considerably ( $P < 0.05$ ) for all gaps larger than the reference gap [Fig. 13(b)].

The backscatter increases with the number of scattering particles and consequently with the size of the gap (Fig. 12). This causes the estimate of all intensity related parameters (e.g.,  $Amp$ ) to increase accordingly. To judge whether the intensity-related parameters also changed as a consequence of the shear-rate decay, we normalized them. Normalization was achieved by calculating the ratio—for each gap—of the parameter of interest and the backscatter intensity during disaggregation ( $I_{dis}$ ). The latter is only affected by the gap width and not by the state of the cells since the disaggregation shear rate (hence, cell elongation) is held constant throughout the gaps. The ratio of each intensity-related parameter and  $I_{dis}$ , therefore, cancels the effect of increased scattering when using larger gaps. Fig. 14 shows the normalized intensity-related parameter estimates, where the values for the 0.37-mm gap were again taken as reference. The figure demonstrates that  $Upstroke/I_{dis}$  (with  $Upstroke = I_{top} - I_{dis}$ ) clearly decreases ( $P < 0.05$ ) with the gap width. The reduced intensity peak

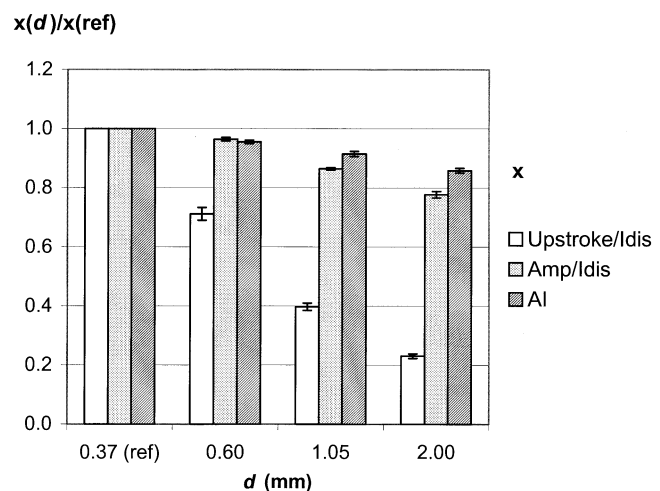


Fig. 14. Changes in intensity parameters compared to the intensity level during disaggregation  $I_{dis}$  in different gaps ( $d$ ). Results of the 0.37-mm gap served as reference. The error bars indicate the standard error or the mean ( $N = 4$  for the 2-mm gap,  $N = 8$  for all other gaps).

decreases ( $P < 0.05$ ) the extent of aggregation ( $Amp$ ) and the  $AI$  for all gaps larger than 0.37 mm although the effect is relatively small for the 0.6-mm gap. This finding proves that it is incorrect to compare the  $Amp$  and  $AI$  values between aggregometers with different gap widths.

#### IV. DISCUSSION

This paper studied the influence of aggregometer-geometry dependent shear-rate decay on the shape of the syllectogram. Based on the Navier–Stokes equations a complete mathematical model of the velocity and shear-rate decay is presented. The flow-decay model was calculated for the parallel plate geometry but describes the general concept, which applies to virtually any aggregometer. We also propose an improved mathematical representation of the syllectogram that includes the upstroke ascribed to RBC-shape recovery. This representation is used to quantify the effect of prolonged shear-rate decay on RBC-shape recovery and aggregation parameters.

The mathematical model of the velocity decay was validated by experiment and reveals that the shear rate is not uniformly distributed over the gap after cup cessation. This causes RBCs in close vicinity of the bob to be in a different state of shape recovery and aggregation than distant RBCs. Clearly, the backscatter intensity is a composite signal that depends not only on the number of scattering cells but also on the state of these cells. This finding confirmed our expectation that the shape of the syllectogram and many of its derived parameters depend on the gap width.

The experiments showed that the triexponential syllectogram representation performs well in fitting the complete aggregation curve of normal human blood, including the upstroke. For the 2-mm gap, however, the upstroke shows up with a slight delay causing a mismatch of the curve fit. This delay is well explained by the prolonged shear-rate decay time that exceeds the RBC-shape recovery time.

Using the triexponential syllectogram representation, we showed that many RBC-shape recovery and aggregation parameters changed considerably in gaps larger than 0.6

mm as a consequence of prolonged shear-rate decay: The shape recovery time-constant  $T_r$  is clearly increased and the occurrence of intensity peak  $t_{\text{top}}$  is delayed. The *upstroke* following cup cessation is relatively small for large gaps. This is the reason why the extent of aggregation ( $Amp$ ) and the AI are underestimated in the case of larger gaps. The reduced upstroke also causes the half-life parameter ( $t_{1/2}$ ) to increase considerably in large gaps ( $>0.6$  mm).

The use of small gaps in aggregation measurements is sometimes criticized because of the limited space available for 3-D aggregate formation [11]. In pathological cases, aggregates of 500  $\mu\text{m}$  may appear [12]. Our results with blood of healthy volunteers show relatively small differences in the aggregation time-constants attributable to rouleaux formation ( $T_f$ ) and 3-D aggregate formation ( $T_s$ ), which allows comparing only these two parameters between aggregometers with different gap widths.

The RBC-shape recovery time-constant of  $59 \pm 6$  ms found after shearing blood at  $400 \text{ s}^{-1}$  in a 0.37-mm gap agrees with the value ( $62 \pm 12$  ms) found by Baskurt and Meiselman [20] for RBCs in a Dextran medium of comparable viscosity. Their experiments show a relatively large oscillation in the first 150 ms following cup cessation probably caused by: 1) the higher mass of the commercial LORCA cup compared to our Plexiglas cup, and 2) the absence of an additional brake mechanism. If the repetition interval of the oscillation is short (relatively fast oscillation) compared to the shape recovery time-constant, the triexponential curve is fitted fluently through the oscillation with negligible deviation. If, however, the repetition interval of the oscillation is long and close to the shape recovery time-constant, ringing will influence the shape of the syllectogram peak resulting in a deviation of the fit.

Our new approach for determining RBC-shape recovery in whole blood using the triexponential syllectogram representation is more physiological and considerably simplifies the measurement. Moreover, it prevents modification of RBC properties caused by washing and re-suspension in artificial media.

## V. CONCLUSION

Modeling the velocity and shear-rate decay provided important insight into the physics involved in syllectometry using Couette aggregometers. The shear rate following cup cessation is not uniformly distributed over the gap, which causes cells to be in different states of shape recovery and aggregation. The increased mass inertia of the suspension prolongs the shear-rate decay and increases the apparent RBC-shape recovery time-constant for large gaps. These facts cause the syllectogram to be gap-width dependent. As a result most RBC-shape recovery and aggregation parameters change considerably in gaps larger than 0.6 mm. Thus, for accurate syllectogram measurements a gap width of up to 0.6 mm is recommended.

The novel triexponential syllectogram representation performs better than conventional biexponential representations, especially in the first few seconds of the measurement. This results in an improved accuracy of the parameters describing the syllectogram. With the addition of the new shape-recovery term, it is now possible to measure the time-constant describing RBC-shape recovery in whole blood as well.

## APPENDIX

### CALCULATION OF THE VELOCITY AND SHEAR-RATE DECAY

To calculate the decay of the velocity profile, we assume a Newtonian fluid and the initial flow ( $t \leq 0$ ) laminar and 1-D with a velocity component in the  $x$ -direction only. Provided that the gap is small in relation to the bob radius, the velocity profile in a parallel plate system [Fig. 2(a)] approximates that in a Couette geometry. Under these assumptions the Navier–Stokes equations reduce to a single, second-order partial differential equation

$$\frac{\partial u(y, t)}{\partial t} = v \frac{\partial^2 u(y, t)}{\partial y^2} \quad (\text{A1})$$

with  $v$  the kinematic viscosity ( $v = \eta/\rho$ ,  $\eta$ : dynamic fluid viscosity,  $\rho$ : fluid density). For ( $t \leq 0$ ) the velocity alters proportionally with the position  $y$  between the plates and accordingly we take as initial condition  $u(y, t) = \gamma_0 \cdot y$ , with  $\gamma_0$  the initial shear rate. When at  $t = 0$  the cup stops, mass inertia causes the fluid to stop slightly retarded. For the initial and the boundary conditions we, thus, have

$$u(y, 0) = \gamma_0 y \quad (\text{A2})$$

$$u(0, t) = 0 \quad (t \geq 0) \quad (\text{A3a})$$

$$u(d, t) = 0 \quad (t \geq 0) \quad (\text{A3b})$$

with  $d$  the position of the outer border (gap width). If cup cessation is followed by oscillatory motion, (A3b) has to be replaced by

$$u(d, t) = \frac{d}{dt} \left[ A e^{-t/t_c} \text{Sin}[\omega \cdot t] \right]. \quad (\text{A3c})$$

In (A3c),  $A$  and  $\omega$  describe the initial amplitude and radial frequency of the oscillatory motion while  $t_c$  represents the time-constant associated with the oscillatory motion decay.

Under the conditions (A2)–(A3b), i.e., no oscillatory cup cessation, the solution for this differential equation can be obtained using Laplace transformation; the procedures and the solution(s) are fully described in reference [22]

$$u(y, t) = \gamma_0 \frac{d}{\pi} \sum_{n=1}^{\infty} \frac{a(n)}{n} \quad \text{with} \quad (\text{A4a})$$

$$a(n) = 2 \cdot (-1)^n \sin\left(\frac{n\pi y}{d}\right) \cdot e^{-\left(\frac{n\pi}{d}\right)^2 vt}. \quad (\text{A4b})$$

To solve the differential equation with the oscillatory boundary condition, we also made use of the Laplace transformation. First (A1) was transformed, incorporating the initial condition (A2). With  $u(y, t) \Rightarrow U(y, s)$ , (A1) transforms into:

$$\frac{d^2 U(y, s)}{dy^2} - v \{ s U(y, s) - \gamma_0 y \} = 0. \quad (\text{A5})$$

Likewise the boundary (A3a) and (A3c) were transformed

$$U(0, s) = 0 \quad (\text{A6a})$$

$$U(d, s) = \frac{A t_c^2 \omega s}{1 + 2t_c s + t_c^2 s^2 + t_c^2 \omega^2}. \quad (\text{A6b})$$

Equation (A5) was solved using the method of variation of parameters. Introducing (A6a) and (A6b) as boundary conditions

$$u(y, t) = -\gamma_0 \frac{d}{\pi} \sum_{n=1}^{\infty} \frac{a(n)}{n} \quad (\text{A8a})$$

$$+ A \frac{\pi^3 v^2 t_c^2 \omega}{d^4} \sum_{n=1}^{\infty} \frac{a(n) \cdot n^3}{\left(1 - 2 \left(\frac{n\pi}{d}\right)^2 v \cdot t_c + \left(\frac{n\pi}{d}\right)^4 (v \cdot t_c)^2 + (t_c \omega)^2\right)} \quad (\text{A8b})$$

$$+ \frac{A}{t_c} \text{Re} \left[ (i + t_c \omega) \cdot e^{t((1/t) + i \cdot \omega)} \cdot \frac{\text{Sinh} \left[ y \sqrt{\frac{1}{v} \left(-\frac{1}{t_c} + i \cdot \omega\right)} \right]}{\text{Sinh} \left[ d \sqrt{\frac{1}{v} \left(-\frac{1}{t_c} + i \cdot \omega\right)} \right]} \right] \quad (\text{A8c})$$

$$\gamma(y, t) = -\gamma_0 \sum_{n=1}^{\infty} b(n) \quad (\text{A9a})$$

$$+ A \frac{\pi^4 v^2 t_c^2 \omega}{d^5} \sum_{n=1}^{\infty} \frac{b(n) \cdot n^4}{\left(1 - 2 \left(\frac{n\pi}{d}\right)^2 v \cdot t_c + \left(\frac{n\pi}{d}\right)^4 (v \cdot t_c)^2 + (t_c \omega)^2\right)} \quad (\text{A9b})$$

$$+ \frac{A}{t_c} \text{Re} \left[ (i + t_c \omega) \cdot \sqrt{\frac{1}{v} \left(-\frac{1}{t_c} + i \cdot \omega\right)} e^{t((1/t) + i \cdot \omega)} \cdot \frac{\text{Cosh} \left[ y \sqrt{\frac{1}{v} \left(-\frac{1}{t_c} + i \cdot \omega\right)} \right]}{\text{Sinh} \left[ d \sqrt{\frac{1}{v} \left(-\frac{1}{t_c} + i \cdot \omega\right)} \right]} \right] \quad (\text{A9c})$$

$$\text{with: } b(n) = 2 \cdot (-1)^n \cos \left( \frac{n\pi y}{d} \right) \cdot e^{-\left(\frac{n\pi}{d}\right)^2 v t} \quad (\text{A9d})$$

resulted in

$$U(y, s) = \frac{\gamma_0 y}{s} - \frac{d\gamma_0 \text{Sinh}(y\sqrt{\frac{s}{v}})}{s \text{Sinh}(d\sqrt{\frac{s}{v}})} + \frac{At_c^2 \omega s \text{Sinh}(y\sqrt{\frac{s}{v}})}{(1 + 2t_c s + t_c^2 s^2 + t_c^2 \omega^2) \text{Sinh}(d\sqrt{\frac{s}{v}})} \quad (\text{A7})$$

The inverse Laplace transformation of the first two terms of  $U(y, s)$  produced the solution without ringing, i.e., (A4a). For the inverse transformation of the third term its poles (= zeros of the denominator) were computed and from these values with help of Mathematica version 4.0 (Wolfram Research, Champaign, IL) the appropriate residues. For the complete solution of the differential equation with an oscillatory boundary condition we, thus, have (A8a)–(A8c), shown at the top of the page.

With  $a(n)$  as defined under (A4b). From this equation, the shear rate  $\gamma(y, t)$  follows as the partial derivative of  $u(y, t)$  to  $y$  as shown in (A9a)–(A9d) at the top of the page.

Again, the terms (A9b) and (A9c) cover the effect of oscillatory cup cessation and should be omitted if the cup stops instantly.

#### ACKNOWLEDGMENT

The authors would like to thank A. J. Danner for creating the Plexiglas cups, D. Ramsoekh and S. Harkisoen for performing clinical experiments with the LORCA and Dr. M. R. Hardeman for helpful discussions on RBC aggregation.

#### REFERENCES

[1] H. Zhao, X. Wang, and J. F. Stoltz, "Comparison of three optical methods to study erythrocyte aggregation," *Clin. Hemorheol. Microcirc.*, vol. 21, pp. 297–302, 1999.

[2] W. G. Zijlstra, "Syllectometry, a new method for studying rouleaux formation of red blood cells," *Netherlands Soc. Physiol. Pharmacol.*, vol. 8, pp. 153–154, Oct. 1957.

[3] R. Brinkman, W. G. Zijlstra, and N. J. Jansonius, "Quantitative evaluation of the rate of rouleaux formation of erythrocytes by measuring light reflection ("Syllectometry")," *Proc. Roy. Dutch Academy Science, Series C*, vol. 66, no. 3, pp. 236–247, Jan. 1963.

[4] H. Schmid-Schonbein, J. van Gosen, L. Heinrich, H. J. Klose, and E. Volger, "A counter-rotating "rheoscope chamber" for the study of the micro rheology of blood cell aggregation by microscopic observation and microphotometry," *Microvasc. Res.*, vol. 6, pp. 366–376, 1973.

[5] J. F. Stoltz and M. Donner, "Erythrocyte aggregation: Experimental approaches and clinical implications," *Int. Angiol.*, vol. 6, pp. 193–201, 1987.

[6] F. J. Neumann, H. Schmid-Schonbein, and H. Ohlenbusch, "Temperature-dependence of red cell aggregation," *Eur. J. Physiol.*, vol. 408, pp. 524–530, 1987.

[7] M. Donner, M. Siadat, and J. F. Stoltz, "Erythrocyte aggregation: Approach by light scattering determination," *Biorheology*, vol. 25, no. 1/2, pp. 367–375, 1988.

[8] R. M. Bauersachs, R. B. Wenby, and H. J. Meiselman, "Determination of specific red blood cell aggregation indices via an automated system," *Clin. Hemorheol.*, vol. 9, pp. 1–25, 1989.

[9] M. R. Hardeman, P. T. Goedhart, J. G. G. Dobbe, and K. P. Lettinga, "Laser-assisted optical rotational cell analyzer (LORCA); a new instrument for measurement of various structural hemorheological parameters," *Clin. Hemorheol.*, vol. 14, no. 4, pp. 605–618, 1994.

[10] N. N. Firsov, A. Bjelle, T. V. Korotaeva, A. V. Priezhev, and O. M. Ryaboshapka, "Clinical application of the measurement of spontaneous erythrocyte aggregation and disaggregation. A pilot study," *Clin. Hemorheol. Microcirc.*, vol. 18, pp. 87–97, 1998.

[11] A. V. Priezhev, O. M. Ryaboshapka, N. N. Firsov, and I. V. Sirko, "Aggregation and disaggregation of erythrocytes in whole blood: Study by backscattering technique," *J. Biomed. Opt.*, vol. 4, no. 1, pp. 76–84, Jan. 1999.

[12] J. Lademann, H. G. Weigmann, W. Sterry, A. Roggan, G. Muller, A. V. Priezhev, and N. N. Firsov, "Investigation of the aggregation and disaggregation properties of erythrocytes by light scattering measurements," *Laser Phys.*, vol. 9, no. 1, pp. 357–362, 1999.

[13] A. Gaspar-Rosas and G. B. Thurston, "Erythrocyte aggregate rheology by transmitted and reflected light," *Biorheology*, vol. 25, pp. 471–487, 1988.

- [14] R. Fahraeus, "The suspension stability of the blood," *Physiol. Rev.*, vol. 9, no. 2, pp. 241–274, 1929.
- [15] H. L. Reid, A. J. Barnes, P. J. Lock, J. A. Dormandy, and T. L. Dormandy, "A simple method for measuring erythrocyte deformability," *J. Clin. Pathol.*, vol. 29, pp. 855–858, 1976.
- [16] R. J. Zdrojkowski and N. R. Pisharoty, "Optical transmission and reflection by blood," *IEEE Trans. Biomed. Eng.*, vol. BME-17, pp. 122–128, Apr. 1970.
- [17] A. K. Prasad, "Particle image velocimetry," *Curr. Sci.*, vol. 79, no. 1, pp. 51–60, July 2000.
- [18] S. Chien and L. A. Sung, "Physicochemical basis and clinical implications of red cell aggregation," *Clin. Hemorheol.*, vol. 7, pp. 71–91, 1987.
- [19] F. M. White, "The differential equation of linear momentum," in *Fluid Mechanics (Paragraph 4.3)*, 4th ed. New York: McGraw-Hill, 1999, pp. 223–230.
- [20] O. K. Baskurt and H. J. Meiselman, "Determination of red blood cell shape recovery time constant in a couette system by the analysis of light reflectance and ektacytometry," *Biorheology*, vol. 33, no. 6, pp. 489–503, 1996.
- [21] W. H. Press, A. A. Teukolsky, W. T. Vetterling, and B. P. Flannery, "Levenberg-Marquardt method," in *Numerical Recipes in C*, 2nd ed. Cambridge, U.K.: Cambridge Univ. Press, 1992, The art of scientific computing, pp. 683–688.
- [22] H. S. Carslaw and J. C. Jaeger, "Linear flow of heat in the solid bounded by two parallel planes," in *Conduction of Heat in Solids*, 2nd ed. Oxford, U.K.: Clarendon, 1959, ch. 3, pp. 92–99.



**Johannes G. G. Dobbe** was born in Amsterdam, The Netherlands, in 1964. He received the B.Sc. degree in electrical engineering and the Ph.D. degree for "Engineering developments in hemorheology," from the University of Amsterdam in 1987 and 2002, respectively.

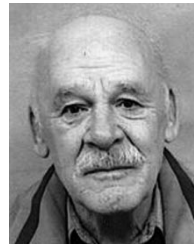
Since 1987, he has been with the Academic Medical Center of the University of Amsterdam, serving as engineer in the development of medical instruments. Most of the time he is writing software for laboratory automation and for medical research.



**Geert J. Streekstra** was born in Kampen, The Netherlands, in 1961. He received the M.S. degree in physics from the University of Twente, Twente, The Netherlands, in 1988. The subject of his masters thesis is the rheology of saliva and saliva substitutes. He received the Ph.D. degree in red blood cell rheology at Utrecht University, The Netherlands, in 1994.

After receiving the Ph.D. degree he started a Post Doc position at the Department of Physiology and Biophysics, University of Southern California, Los Angeles. In the lab of Prof. Dr. H. J. Meiselman, he worked on the development of an optical method for the detection of poorly deformable red blood cells from sickle cell patients. In 1995, he moved to Utrecht, The Netherlands, and worked on coronary bypass surgery on the beating heart. In the Department of Cardiology and Cardiac Surgery, he developed principles for automated bypass grafting methods for cardiac surgery. In 1997, he joined the Intelligent Sensory Information Systems group at the University of Amsterdam where he developed 3-D image processing methods for the analysis of neuronal structures from confocal images. Since 2000, he is Assistant Professor at the Medical Physics department of the Academic Medical Center, Amsterdam. His main research interests are medical imaging and red blood cell rheology.

Dr. Streekstra received the Instrumentation Award at the 9th International Congress of Biorheology, Big Sky, Montana, in 1995.



**Jan Strackee** was born in Amsterdam, the Netherlands, in 1924. He was trained as a physicist at the University of Amsterdam, where he received the Ph.D. degree on cosmic ray research in 1951.

He started his career as Research Physicist with the Medical Faculty of the University of Amsterdam where he soon became interested in signal analysis of the EEG and ECG. In the 1960s, he gradually switched to computer science and in 1973 became full Professor of Medical Informatics. His main interests were 3-D image processing and the statistical aspects of signals of biological material. He retired in 1989.



**Marcel C. M. Rutten** was born in St-Hubert, The Netherlands, in 1963. He received the M.S. degree in mechanical engineering from the Eindhoven University, Eindhoven, The Netherlands, in 1993 and the Ph.D. on fluid structure interaction in large arteries in 1998.

Since then, he is a Lecturer in cardiovascular mechanics in the Department of Biomedical Engineering at Eindhoven University.



**Johannes M. A. Stijnen** was born in Geleen, The Netherlands, in 1973. He received the M.S. degree in mechanical engineering from the Eindhoven University of Technology, Eindhoven, The Netherlands, in 1998. He is working towards the Ph.D. degree in study of the influence of prosthetic mitral valve orientation on the left heart ventricle function and flow phenomena at the Department of Biomedical Engineering, the Eindhoven University of Technology. His Ph.D study will be completed in 2003.



**Cornelis A. Grimbergen** was born in 1947. He received the Ir. degree in electrical engineering from Delft University of Technology (DUT), Delft, The Netherlands, in 1971 and the Ph.D. degree in solid state physics from the University of Groningen, Groningen, The Netherlands, in 1977.

Since 1977, he has been an Assistant Professor in the Laboratory of Medical Physics, the University of Amsterdam, Amsterdam, The Netherlands. He is part-time Professor in the Measurement & Control Department of the DUT and Professor in Medical Technology at the Academic Medical Center of the University of Amsterdam. His interests are medical instrumentation, biomedical signal and image processing, and minimally invasive techniques.